

# Astrophysical searches for a hidden-photon signal in the radio regime

Andrei P. Lobanov\*

*Max-Planck-Institut für Radioastronomie, Auf dem Hügel 69, 53121 Bonn, Germany*<sup>†</sup>

Hannes-S. Zechlin<sup>‡</sup> and Dieter Horns<sup>§</sup>

*University of Hamburg, Institut für Experimentalphysik,  
Luruper Chaussee 149, D-22761 Hamburg, Germany*

(Dated: November 26, 2012)

Common extensions of the Standard Model of particle physics predict the existence of a “hidden” sector that comprises particles with a vanishing or very weak coupling to particles of the Standard Model (visible sector). For very light ( $m < 10^{-14}$  eV) hidden U(1) gauge bosons (hidden photons), broad-band radio spectra of compact radio sources could be modified due to weak kinetic mixing with radio photons. Here, search methods are developed and their sensitivity discussed, with specific emphasis on the effect of the coherence length of the signal, instrumental bandwidth, and spectral resolution. We conclude that radio observations in the frequency range of 0.03–1400 GHz probe kinetic mixing of  $\sim 10^{-3}$  of hidden photons with masses down to  $\sim 10^{-17}$  eV. Prospects for improving the sensitivity with future radio astronomical facilities as well as by stacking data from multiple objects are discussed.

## I. INTRODUCTION

Finding experimental evidence for physics beyond the Standard Model (SM) of particle physics is one of the pinnacles of present-day physical research, embracing both extensive laboratory studies and indirect (primarily) astrophysical measurements made across a very broad range of energies. Most of present-day SM extensions into a more generic, unified scenario predict existence of a class of particles only weakly interacting with the normal matter: weakly interacting massive particles (WIMP) at a mass scale of  $\mathcal{O}(100)$  GeV [1–3] and ultralight weakly interacting sub-eV particles (WISP) [4–8].

The existence of ultralight particles has been argued to be at least theoretically plausible in a number of different scenarios including additional pseudo-scalar (axions and axion-like particles (ALP),  $\phi$ , [9–11]) as well as vector fields (U(1) hidden photons,  $\gamma_s$ , [4, 6, 7, 12]). In either scenario, the prevailing non-baryonic matter could be explained by these ultra-light fields [13, 14].

Hidden photons arise in low-energy extensions of the SM which leave all the SM fields uncharged under the additional hidden gauge group. Interaction between hidden photons and massive SM particles is expected to be suppressed by the particle masses. However, it can be manifested by kinetic mixing with normal photons [4, 12, 15]. In low-energy SM extensions with hidden photons, the kinetic mixing is expressed by the effective Lagrangian describing two-photon interactions  $\mathcal{L} = \mathcal{L}_{\text{SM}} + \mathcal{L}_h + \mathcal{L}_\chi$  [*cf.*, 13, 16, 17], with  $\mathcal{L}_{\text{SM}}$  denoting the Maxwell Lagrangian for the SM photon field, the  $\mathcal{L}_h$  term describing

the Proca-Lagrangian for the hidden photon field, and  $\mathcal{L}_\chi$  representing a gauge-invariant kinetic mixing term. The kinetic mixing term induces photon oscillations between the massless “normal” state ( $\gamma$ ) and a non-zero mass “hidden” state ( $\gamma_s$ ). In this hidden state, photons acquire a non-vanishing mass and propagate on space-like geodesics, without any interaction with normal matter. The physical properties of a hidden photon can be completely described by its mass  $m_{\gamma_s}$  and the kinetic mixing with an SM photon (expressed by the mixing angle  $\chi$ ). Theoretical predictions for  $\chi$  are falling in the broad range between  $10^{-16}$  and  $10^{-2}$  [15, 18–22].

Accelerator experiments are generally optimized to search for new heavy particles such as WIMPs, and therefore of limited sensitivity and mass reach for WISPs. Hence, the potential discovery of ultralight particles requires high-precision experiments for which non-accelerator setups often appear more promising [23–25].

Evidence for the  $\gamma$ – $\gamma_s$  oscillations has been searched for in a number of laboratory [26–31] and astrophysical experiments [7, 17, 28, 32–35], focusing in particular on “light shining through the wall” (LSW, [36]) experiments such as ALPS [27] and searches for hidden photons from the Sun (SHIPS; [28, 37]). The non-detection of hidden-photon signals has so far yielded strong bounds on the kinetic mixing parameter  $\chi$  for a broad range of hidden photon masses [6, 7, 14, and references therein]. The mass range which has been currently probed extends down to  $m_{\gamma_s} = 2 \times 10^{-14}$  eV, with the lowest hidden-photon masses probed by the WMAP CMB measurements in the radio domain at frequencies above 22 GHz [33]. Below  $10^{-14}$  eV, only weak limits of  $\chi \approx 10^{-2}$  [6] have been obtained from analysis of early measurements of magnetic field around Earth and Jupiter [38], and no limits are reported for  $m_{\gamma_s} \lesssim 5 \times 10^{-16}$  eV.

Radio observations at frequencies below 22 GHz offer an excellent (if not unique) tool for placing bounds on the mixing angle  $\chi$  for  $m_{\gamma_s} < 10^{-14}$  eV. Initial bounds

\* alobanov@mpifr-bonn.mpg.de

<sup>†</sup> Visiting Scientist, University of Hamburg / Deutsches Elektronen Synchrotron (DESY) Forschungszentrum

<sup>‡</sup> hzechlin@physik.uni-hamburg.de

<sup>§</sup> dieter.horns@physik.uni-hamburg.de

on  $\chi$  can be obtained from existing radio data on compact, weakly variable objects with well-known radio spectra (such as young supernova remnants (SNR), planetary nebula, and steep spectrum radio sources typically used for the absolute flux density calibration of radio telescopes). With this approach, one can reasonably expect to reach  $\chi \lesssim 0.01$ . Propagation through a refractive medium (in which an SM photon also acquires an effective mass  $m_\gamma$ ) can strongly affect this limit, improving it substantially near the resonance condition  $m_{\gamma_s} = m_\gamma$ , and suppressing the hidden photon conversion at  $m_\gamma \gg m_{\gamma_s}$  [33]. The latter effect can become important at  $m_{\gamma_s} \lesssim 10^{-15}$  eV.

Placing better bounds on  $\chi$  can now be achieved by using the expanded capabilities of existing radio telescopes (utilizing the upgraded broad-band coverage and spectral resolution of the Effelsberg 100-meter antenna and the Karl Jansky Very Large Array (JVLA) in the 0.3–40 GHz frequency range), by extending the measurements both to lower frequencies (0.03–0.3 GHz) covered by the Low Frequency Array (LOFAR) and to submillimeter wavelengths probed by Atacama Large Millimeter Array (ALMA), and by employing the superb brightness sensitivity ( $\sim 1 \mu\text{Jy}$  [39]) of the SKA[40] and its precursors, MeerKAT[41] and ASKAP[42].

The existing data for the primary absolute flux density calibrators in the radio regime (such as Cas A, Tau A, and Cyg A) [43] feature a few dozens of absolute flux density measurements made in the 0.01–30 GHz spectral range and reaching a  $\sim 3$ –5% accuracy. These data should enable placing a bound of  $\chi \approx 0.02$ , from measurements of the r.m.s. of deviations from a canonical source spectrum. If the spectral resolution is sufficiently high to assess the periodicity in the oscillation signal (particularly at the lower end of the spectrum), both the limits on  $\chi$  and the range of photon mass studied can be improved. Further improvements of the bounds on  $\chi$  can be achieved by stacking the signal from a number of objects, under the condition that the observations of different objects are sensitive to the same range of the hidden-photon mass.

In this paper, a methodology and prospects for detection of the hidden photon signal in the radio regime are considered. The basic physics of the  $\gamma - \gamma_s$  oscillation and the propagation of the hidden-photon signal are described in Section II. Methods for the detection of the oscillation signal with different instruments and targets are discussed in Section III and potentials of these studies are discussed in Section IV.

## II. PHOTON OSCILLATIONS IN THE RADIO REGIME

For a photon field,  $A_\mu$ , and a hidden photon field,  $B_\mu$ , the kinetic mixing term is given by [16]

$$\mathcal{L}_\chi = \frac{\sin \chi}{2} A_{\mu\nu} B^{\mu\nu} + \frac{\cos^2 \chi}{2} m_{\gamma_s}^2 B_\mu B^\mu, \quad (1)$$

where  $A_{\mu\nu}$  and  $B_{\mu\nu}$  are the respective field-strength tensors. The non-zero kinetic mixing angle  $\chi$  implies a mismatch between the interaction and propagation eigenstates, which induces oscillation between the two states (with a close analogy to the neutrino oscillation effect [44]). The last term accounts for massive hidden photons via Higgs or Stückelberg mechanisms, where the former case suffers from additional constraints [6]. The probability of the  $\gamma \rightarrow \gamma_s$  conversion after propagating a distance  $L$  in vacuum is then given by

$$P_{\gamma \rightarrow \gamma_s}(L) = a_\chi \sin^2 \left( \frac{m_{\gamma_s}^2 L}{4E} \right) = a_\chi \sin^2 \left( \frac{m_{\gamma_s}^2 L}{8\pi\nu} \right), \quad (2)$$

where all quantities are expressed in natural units, and  $E$  and  $\nu$  are the energy and frequency of the normal photon [12, 16, 32]. It should be noted that the validity of Eq. 2 is restricted to the case of  $m_{\gamma_s} \ll 2\pi\nu$ , which is fulfilled for all considerations in this paper.

The first term of Eq. 2 describes the amplitude of the oscillation,  $a_\chi = \sin^2(2\chi) \approx 4\chi^2$  (for  $\chi \ll 1$ ), that can be identified as a periodic signal over a range of distances  $L$  or wavelengths  $\lambda = 1/\nu$ . The second term,

$$\varphi_{\gamma_s}(\nu) = \frac{m_{\gamma_s}^2 L}{8\pi\nu} = 9.45 \left( \frac{m_{\gamma_s}}{10^{-15} \text{ eV}} \right)^2 \left( \frac{L}{\text{pc}} \right) \left( \frac{\nu}{\text{MHz}} \right)^{-1}, \quad (3)$$

gives the periodic signature of the oscillation. The oscillation signal affects the broad-band spectrum,  $F(\nu)$ , of an astrophysical source, which results in a received spectrum  $F_{\gamma_s}(\nu) = F(\nu) (1 - P_{\gamma \rightarrow \gamma_s})$ .

The resulting spectrum  $F_{\gamma_s}(\nu)$  will have local minima and maxima at the frequencies  $\nu_{\min,i} = \nu_\star / (2i - 1)$  and  $\nu_{\max,i} = \nu_\star / (2i)$ ,  $i \in \mathbb{N}$ , where

$$\nu_\star = \frac{m_{\gamma_s}^2 L}{4\pi^2} = 6.02 \left( \frac{m_{\gamma_s}}{10^{-15} \text{ eV}} \right)^2 \left( \frac{L}{\text{pc}} \right) \text{ MHz} \quad (4)$$

is the frequency of the first (highest frequency) minimum obtained with  $i = 1$ . The frequency,  $\nu_{\max,1}$ , of the first maximum defines the characteristic wavelength,

$$\lambda_\star = \frac{8\pi^2}{m_{\gamma_s}^2 L} = 99.64 \left( \frac{m_{\gamma_s}}{10^{-15} \text{ eV}} \right)^{-2} \left( \frac{L}{\text{pc}} \right)^{-1} \text{ m} \quad (5)$$

of the periodic modulation induced by the hidden-photon signal on a broad-band spectrum  $F(\lambda)$  in the wavelength domain.

### A. Oscillation and coherence lengths

The oscillation length of the hidden-photon signal is set by the condition  $\varphi_{\gamma_s}(L, \nu) = \pi$ ,

$$L_{\text{osc}} = 0.33 \left( \frac{\nu}{\text{MHz}} \right) \left( \frac{m_{\gamma_s}}{10^{-15} \text{ eV}} \right)^{-2} \text{ pc}. \quad (6)$$

Decoherence effects in the photon and hidden-photon mass eigenstates may arise during propagation, owing to

the finite mass,  $m_{\gamma_s}$ , of the latter. An accurate quantum mechanical treatment of the oscillation probability  $P_{\gamma \rightarrow \gamma_s}$  using wave packets (Eq. 2 has been derived assuming plane waves) yields an upper bound on the accessible distance range [32, 45, 46],  $L_{\text{coh}} = 4\sqrt{2}\sigma_x E^2/m_{\gamma_s}^2$ , where  $\sigma_x^2 = \sigma_x^P{}^2 + \sigma_x^D{}^2$  denotes the quantum mechanical uncertainties of the production and detection processes, respectively. The non-thermal radio emission of compact radio sources is produced by synchrotron radiation, with the mean energy loss path of synchrotron emitting electrons  $\sigma_x^P = \Delta\tau$  (note that the mean energy loss path is of the same order of magnitude as the gyro radius of the relativistic electrons under consideration). A reasonable estimate of the cooling time  $\Delta\tau = 2\pi\nu_c/(-dE/dt)$  can be obtained at the critical frequency  $\nu_c$  of synchrotron radiation (averaging over the pitch angle) [47], eventually yielding

$$L_{\text{coh}} = 19.84 \left(\frac{\nu}{\text{MHz}}\right)^2 \left(\frac{m_{\gamma_s}}{10^{-15} \text{ eV}}\right)^{-2} \left(\frac{B}{\text{mG}}\right)^{-1} \text{ kpc}, \quad (7)$$

where  $B$  denotes the magnetic field inside the considered source. To avoid a freeze out of vacuum  $\gamma - \gamma_s$  oscillations, the probed distance  $L$  therefore needs to fulfill the condition  $L_{\text{osc}} \leq L \leq L_{\text{coh}}$ .

Together with the condition  $L_{\text{osc}} \leq L \leq L_{\text{coh}}$ , Eqs. 6 and 7 imply effective lower and upper bounds on the hidden-photon mass that can be probed with radio data of a compact synchrotron emitting source at distance  $L_0$  above a given frequency  $\nu_0$ . Table I lists corresponding bounds considering three distinct types of radio sources, namely nearby Galactic supernova remnants (SNR), distant radio-emitting lobes of active galactic nuclei (AGN), and AGN cores at cosmological distance scales. It demonstrates that the oscillation length and decoherence effects should enable effective radio measurements for a range of hidden-photon masses between  $\sim 3 \times 10^{-19}$  eV and  $\sim 4 \times 10^{-11}$  eV.

## B. Propagation through refractive media

Photon propagation through a medium with refractive index  $n$  can be described by introducing an effective photon mass  $m_\gamma$  to the Lagrangian  $\mathcal{L}$ . This operation affects the kinetic mixing term, and the resulting effective mixing angle  $\chi_r$  depends on the mass ratio  $\xi = m_\gamma^2/m_{\gamma_s}^2$  so that [16, 17, 33]

$$\sin 2\chi_r = \frac{\sin 2\chi}{\sqrt{\sin^2 2\chi + (\cos 2\chi - \xi)^2}}. \quad (8)$$

For small effective photon masses,  $\xi \ll 1$ , the  $\gamma - \gamma_s$  oscillations approach the vacuum regime, with  $\chi_r \rightarrow \chi$ . A resonance with the maximum amplitude  $\chi_r = \pi/4$  of the oscillations is reached at the resonant mass ratio  $\xi = \cos 2\chi$ . For higher effective photon masses,

$m_\gamma$ , the oscillations are rapidly damped (medium suppression), with  $\chi_r \rightarrow \pi/2$  for  $\xi \gg 1$ . The condition  $\sin 2\chi_r \geq \sin 2\chi$  implies that hidden photons with  $m_{\gamma_s}$  and  $\chi$  can be detected in a medium with the effective photon mass  $m_\gamma^2 \leq 2m_{\gamma_s}^2 \cos 2\chi$ , which approximately yields  $m_\gamma \lesssim \sqrt{2}m_{\gamma_s}$  for  $\chi \ll 1$ .

For photon propagation in the interstellar (ISM) and intergalactic (IGM) medium, the dominant factor is scattering off free electrons and neutral atoms (with the medium described by the electron and proton number densities,  $n_e$  and  $n_p$ ). In this case, the effective photon mass,  $m_\gamma^2 \approx \omega_p^2 - 2\omega^2(n-1)_{\text{medium}}$  [33], depends on the photon frequency  $\omega$ , the plasma frequency  $\omega_p^2 = 4\pi\alpha n_e/m_e$ , and the refraction index  $(n-1)_{\text{medium}}$  of the medium.

For Galactic objects and extragalactic objects at small redshifts ( $z < 1$ ), the medium can be assumed strongly ionized (with the ionized fraction of hydrogen  $X_e = n_e/n_p \rightarrow 1$ ). Contributions from helium and heavier elements can be neglected. This yields [33]

$$\begin{aligned} m_\gamma^2 &\approx \omega_p^2 - 2\omega^2(n-1)_{\text{medium}} \\ &\simeq 1.4 \times 10^{-21} \left(\frac{n_p}{\text{cm}^{-3}}\right) \\ &\quad \times \left[X_e - 1.2 \times 10^{-19} \left(\frac{\nu}{\text{MHz}}\right)^2 (1 - X_e)\right] \text{ eV}^2. \end{aligned} \quad (9)$$

For observations in the radio band,  $m_\gamma \approx \omega_p \simeq 3.7 \times 10^{-11} (n_e/\text{cm}^{-3})^{1/2}$  eV provides a good estimate of the effective photon mass under the assumption of  $X_e \approx 1$ . This limits, formally, the hidden-photon mass that can be probed in Galactic and extragalactic objects to  $\sim 10^{-13}$  eV and  $\sim 10^{-14}$  eV, respectively (for generic assumptions for the average densities of  $\tilde{n}_{\text{IGM}} \sim 10^{-5} \text{ cm}^{-3}$  [48] and  $\tilde{n}_{\text{IGM}} \sim 10^{-7} \text{ cm}^{-3}$  [49]). However, both the ISM and the IGM are inhomogeneous, with variations of the density exceeding 2–3 orders of magnitude [50, 51]. Hence, generation and propagation of the hidden-photon signal depend on the line-of-sight (LOS) properties of the medium and its inhomogeneities.

## C. Effects of inhomogeneous media

In an inhomogeneous medium, the minimum value of  $m_{\gamma_s}$  without medium damping is limited by the electron density of underdense regions with  $n_e \ll \tilde{n}_e$ . The traversed underdense region needs to be sufficiently extended to affect the propagation, such that the LOS path-length,  $l_{\text{los}}$ , in these regions is  $l_{\text{los}} \gg L_{\text{osc}}$  (for observations in the radio domain at  $\nu \gtrsim 100$  MHz, this effectively limits  $m_{\gamma_s} \gtrsim 10^{-16}$  eV for Galactic objects, while permitting probing hidden photons with  $m_{\gamma_s} \gtrsim 10^{-19}$  eV with extragalactic targets, see Table I). The resulting spectral pattern after propagating through underdense regions remains “frozen” during subsequent propagation through denser regions (where  $m_{\gamma_s} \gtrsim 2.6 \times 10^{-11} (n_e/\text{cm}^{-3})^{1/2}$ ),

TABLE I. Lower and upper bounds on the mass range of hidden photons,  $m_{\gamma_s}^\ell$  and  $m_{\gamma_s}^u$ , respectively, detectable with radio data ( $\nu > 1$  GHz) of SNR and AGN. For  $m_{\gamma_s} < m_{\gamma_s}^\ell$ , no  $\gamma$ - $\gamma_s$  oscillations will arise; for  $m_{\gamma_s} > m_{\gamma_s}^u$ , decoherence effects yield a freeze out of the oscillation signal. The columns  $B$  and  $\Delta L$  list the assumed magnetic field and distance range, respectively.

Source class	$B$ [mG]	$\Delta L$	$m_{\gamma_s}^\ell$ [eV]	$m_{\gamma_s}^u$ [eV]
SNR	0.1	1–10 kpc	$2 \times 10^{-16} - 6 \times 10^{-16}$	$1 \times 10^{-11} - 4 \times 10^{-11}$
AGN: Radio lobes	1	0.02–3 Gpc	$3 \times 10^{-19} - 4 \times 10^{-18}$	$3 \times 10^{-15} - 3 \times 10^{-14}$
AGN: Nuclear regions	$10^3$	0.02–3 Gpc	$3 \times 10^{-19} - 4 \times 10^{-18}$	$10^{-16} - 10^{-15}$

as both direct and reverse photon conversions are suppressed there. Therefore, for Galactic objects, the lowest detectable hidden-photon mass would be achieved for photon beams propagating between the Galactic arms, while propagation through cosmic voids would set the lower limit on the hidden-photon mass that can be detected in the broad-band spectra of extragalactic targets.

A density of free electrons  $n_{e,\text{loc}} \approx 0.005\text{--}0.01 \text{ cm}^{-3}$  is measured in the local ISM [52, 53], and there is ample evidence for  $n_e$  to vary strongly across the Galaxy [52, 53], with  $n_e \gtrsim 10 \text{ cm}^{-3}$  near the Galactic center,  $n_e \sim 10^{-2} \text{ cm}^{-3}$  in the spiral arms, and  $n_e \ll 10^{-4} \text{ cm}^{-3}$  above the Galactic disk. In mini “void” regions of  $\sim 1$  kpc in extent and located between the spiral arms [53],  $n_e \lesssim 10^{-6} \text{ cm}^{-3}$  can be found [51], which is similar to the values typically measured in the IGM. Hence, detectability of hidden photon oscillation in Galactic sources should depend strongly on the LOS to a specific target, with likely  $m_{\gamma_s} \gtrsim 10^{-12}$  eV detectable for LOS not crossing the spiral arms, while  $m_{\gamma_s} \gtrsim 10^{-15}$  eV may still be detectable for objects at high galactic latitudes, and the LOS crossing inter-arm plasma and the local “voids”.

The electron and proton densities in different structural components of the IGM can be estimated from observations, i.e., IRAS data [54] and SDSS data [55], as well as detailed numerical simulations of large-scale structures [50, 56, 57]. The SDSS data indicates that the voids have a volume filling factor of 0.62 and a median size of  $17 h^{-1}$  Mpc, and Ref. [50] find the baryonic matter density,  $\Omega_{b,\text{void}} \approx (0.045 \pm 0.015) \Omega_b$ , where  $h = H/(100 \text{ km s}^{-1} \text{ Mpc}^{-1})$  is the dimensionless Hubble constant and  $\Omega_b = 0.046 \pm 0.002$  is the average baryon density in the Universe [58]. Table II summarizes the mass fraction,  $m/m_b$ , the volume fraction,  $V/V_c$ , and the relative density,  $\rho/\rho_b$ , of different IGM components (the warm, warm-hot ionized (WHIM), hot, and void components, measured with respect to the total baryon mass  $m_b$ , density  $\rho_b$ , and the comoving volume  $V_c$ ). Based on these values, one can estimate the electron density in the individual IGM components

$$n_{e,\text{medium}} = X_e \frac{\rho_c \Omega_b}{m_p + X_e m_e} \frac{\rho_{\text{medium}}}{\rho_b}, \quad (10)$$

where  $\rho_c = 3H/(8\pi G)$  is the critical density of the Universe,  $m_p$  and  $m_e$  are the proton and electron masses, and  $G$  denotes the gravitational constant. This yields  $n_{e(\rho_b)} = 2.5 \times 10^{-7} \text{ cm}^{-3}$  and enables calculating  $n_e$

and respective limits on  $m_{\gamma_s}$  for different baryonic matter components as listed in Table II (compiled from the results reported in [50, 54–57]).

TABLE II. Baryonic matter components and hidden photon propagation. Each IGM component is described by the temperature  $T$ , mass fraction  $m/m_b$ , comoving volume fraction  $V/V_c$ , local density relative to the average baryon density  $\rho/\rho_b$ , estimated average electron density  $n_e$ , and resulting minimum detectable hidden-photon mass  $m_{\gamma_s}$  as estimated from the average electron density.

Baryonic component	$T$ [K]	$m/m_b$	$V/V_c$	$\rho/\rho_b$	$n_e$ [ $\text{cm}^{-3}$ ]	$m_{\gamma_s}$ [eV]
Galaxies	$< 10^3$	0.054	0.002	27.0	$6.7 \times 10^{-6}$	$6.7 \times 10^{-14}$
Warm IGM	$< 10^5$	0.350	0.342	1.02	$2.6 \times 10^{-7}$	$1.3 \times 10^{-14}$
WHIM IGM	$< 10^6$	0.471	0.030	15.7	$3.9 \times 10^{-6}$	$5.1 \times 10^{-14}$
Hot IGM	$> 10^6$	0.097	0.006	16.1	$4.0 \times 10^{-6}$	$5.2 \times 10^{-14}$
Voids	$\sim 10^6(?)$	0.028	0.620	0.04	$1.1 \times 10^{-8}$	$2.7 \times 10^{-15}$

In cosmic voids, strong density gradients are observed [55, 59, and references therein], with densities at the void center being at least 2–3 orders of magnitude lower than at the edge of the void. Given the galaxy density as a tracer of the gas density, the density profile of electrons,  $n_e(r')$ , can be calculated from the average radial density profile obtained from the galaxy counts (see Fig. 4–6 in [55]), where  $r' = r/r_{\text{void}}$ , with  $r_{\text{void}}$  denoting the void radius. The profile was normalized to reproduce the void average density reported in [50]. For such a profile, the minimum  $m_{\gamma_s}$  can then be calculated by evaluating  $n_e(r)$  at  $L_{\text{osc}}/2$  (to account propagation on both sides from the center of the void). The resulting values are given in Table III for several typical values of the void size and observing frequencies.

This calculation demonstrates that for the assumptions used here, hidden photons with masses as low as  $\sim 10^{-17}$  eV in principle be probed with astrophysical measurements of targets located behind sufficiently large voids. A more detailed account of ISM/IGM inhomogeneities on generation and propagation of the hidden photon signal would rely on extensive numerical simulations of large scale structures, which is beyond the scope of this paper. In the following discussion, the generic  $m_{\gamma_s}$  limits obtained for Galactic ( $\gtrsim 10^{-15}$  eV) and extragalactic ( $\gtrsim 10^{-17}$  eV) objects will be assumed, while

TABLE III. Minimum detectable hidden-photon mass  $m_{\gamma_s}$  in eV, assuming photon propagation through cosmic voids.

Void $2r_{\text{void}}$ [Mpc]	Observing frequency		
	30 MHz	100 MHz	1 GHz
10	$1.7 \times 10^{-17}$	$2.3 \times 10^{-17}$	$4.1 \times 10^{-17}$
30	$1.3 \times 10^{-17}$	$1.7 \times 10^{-17}$	$3.1 \times 10^{-17}$
100	$9.6 \times 10^{-18}$	$1.3 \times 10^{-17}$	$2.3 \times 10^{-17}$

performing calculations for the  $m_\gamma \leq \sqrt{2} m_{\gamma_s}$  case.

It is interesting to note that the signal from hidden photons with a sufficiently low mass,  $m_{\gamma_s}^{\text{free}}$ , should be unaffected by propagation through a high-density structure with a characteristic size  $l_s$ , for which  $l_s < L_{\text{osc}}$ . This implies  $m_{\gamma_s}^{\text{free}} = 2\pi\sqrt{2}(\nu/l_s)^{1/2}$  and yields, at  $\nu = 1$  GHz,  $m_{\gamma_s}^{\text{free}} \approx 1.3 \times 10^{-16}$  eV for propagation through galaxies ( $l_s \approx 20$  kpc).

### III. DETECTION OF THE OSCILLATION SIGNAL

For measurements in the  $m_\gamma \leq \sqrt{2} m_{\gamma_s}$  regime, the two main factors limiting the sensitivity for a hidden photon signal are the spectral energy distribution of the (typically, multicomponent) astrophysical signal and spectral range covered by the resolution of astronomical instruments. As the hidden-photon signal modulates the astrophysical signal, the latter has to be well understood before attempting to detect the oscillation signal in a broad-band spectrum. The astrophysical signal can be modeled with  $\mathcal{M}(\nu)$ , such that a condition

$$F'_{\gamma_s}(\nu) = F_{\gamma_s}(\nu)/\mathcal{M}(\nu) = C_{\mathcal{M}}(1 - P_{\gamma \rightarrow \gamma_s}) + \sigma_{\text{rms}} \quad (11)$$

is achieved (or approached), where  $C_{\mathcal{M}}$  is a constant (expecting  $C_{\mathcal{M}} \rightarrow 1$ ) and  $\sigma_{\text{rms}}$  is the residual fractional noise due to measurement errors and systematic uncertainties of the fit by  $\mathcal{M}(\nu)$  (with  $\sigma_{\text{rms}} \ll C_{\mathcal{M}}$ ). In the radio regime, measurement errors will be dominated by the system noise and atmospheric/ionospheric fluctuations, while the effect of scattering in interstellar and intergalactic plasma would be orders of magnitude smaller and could be safely neglected. If necessary, the condition  $C_{\mathcal{M}} = 1$  can be achieved by normalizing  $F'_{\gamma_s}(\nu)$  over the observed frequency range (this measure would increase the noise and potentially introduce a bias, but it may be necessary to facilitate subsequent searches for a periodic signal).

The conversion probability  $P_{\gamma \rightarrow \gamma_s}$  is periodic in the wavelength domain, which requires that the model description  $\mathcal{M}(\nu)$  must not contain harmonic terms within a certain frequency range. This range is determined by several specific factors, including the distance to the object and the specific value of  $m_{\gamma_s}$  to be probed. This range is calculated and discussed below.

In the following discussion, it is assumed that the observational setup for a broad-band spectrum measurement can be simplified and characterized by a range  $[\nu_1; \nu_2]$  of frequencies probed with a spectral resolution  $\Delta\nu$  (implying that the flux density measurements are made at average intervals  $\Delta\nu$ ). In general,  $\Delta\nu$  may vary across the frequency range, hence it is used here only in the sense of defining the total number of independent flux density measurements  $N_{\text{mes}} = (\nu_2 - \nu_1)/\Delta\nu$ .

#### A. Effective ranges of frequency and hidden-photon mass

The sensitivity to detect the imprint of the amplitude  $a_\chi$  with a significance of  $n_\sigma$  on an observed radio spectrum with a Gaussian noise  $\sigma_{\text{rms}}$  is given by  $a_\chi = n_\sigma \sigma_{\text{rms}}$  (neglecting for the moment systematic errors resulting from an imperfect model representation,  $\mathcal{M}(\nu)$ , of the astrophysical signal and systematic uncertainties of the measurement process). The highest radio frequency,  $\nu_h$ , useful for recovering the oscillation signal can be estimated from  $P_{\gamma \rightarrow \gamma_s} = \sigma_{\text{rms}}$ , yielding (for  $n_\sigma \geq 1$ , using Eq. 2)

$$\nu_h = \frac{\pi}{2} \frac{\nu_\star}{\arcsin(1/\sqrt{n_\sigma})}, \quad (12)$$

with  $\nu_h = \nu_\star$  at  $n_\sigma = 1$ . At  $n_\sigma \geq 2$ ,  $\nu_h \approx (\pi/2) n_\sigma^{1/2} \nu_\star$  gives an estimate of  $\nu_h$  to within a 10% accuracy.

The lowest frequency,  $\nu_\ell$ , containing a usable response from the oscillation is determined by the spectral spacing,  $\Delta\nu$ . In this case, a conservative estimate of  $\nu_\ell$  is provided by the double of the Nyquist sampling rate,  $f_s$ , of the oscillation signal (this is required to take into account that measurements are made at a fixed set of frequencies and hence no ‘‘phase tuning’’ is feasible). The requirement corresponds to  $\varphi_{\gamma_s}(L, \nu_\ell - \Delta\nu/2) - \varphi_{\gamma_s}(L, \nu_\ell + \Delta\nu/2) = \pi/2$  and yields  $\nu_\ell = \sqrt{\nu_\star \Delta\nu + (\Delta\nu/2)^2} \approx \sqrt{\nu_\star \Delta\nu}$ .

Generic properties of a possible measurement are illustrated in Fig. 1, showing a modulation of an astrophysical signal and the frequencies  $\nu_\ell$  and  $\nu_h$ , as well as the observed frequency range  $[\nu_1; \nu_2]$ .

The characteristic frequencies translate into an accessible mass range extending from  $m_{\gamma_s}^\ell$  to  $m_{\gamma_s}^u$ . The lower limit on the detectable hidden-photon mass  $m_{\gamma_s}^\ell$  is determined by  $L = L_{\text{osc}}(\nu_1)$  (see Section II A), corresponding to  $\nu_1$  set to the frequency of the first local maximum  $\nu_{\text{max},1}$ . This yields

$$\begin{aligned} m_{\gamma_s}^\ell &= 2\sqrt{2}\pi \left(\frac{\nu_1}{L}\right)^{1/2} \\ &= 5.77 \times 10^{-16} \left(\frac{\nu_1}{\text{MHz}}\right)^{1/2} \left(\frac{L}{\text{pc}}\right)^{-1/2} \text{ eV}. \end{aligned} \quad (13)$$

The largest accessible hidden-photon mass  $m_{\gamma_s}^u$  is obtained by setting  $\nu_\ell = \nu_2$ , which gives

$$m_{\gamma_s}^u = \frac{2\pi\nu_2}{(L\Delta\nu)^{1/2}} = \frac{1}{\sqrt{2}} \frac{\nu_2}{\nu_1} \left(\frac{\Delta\nu}{\nu_1}\right)^{-1/2} m_{\gamma_s}^\ell. \quad (14)$$

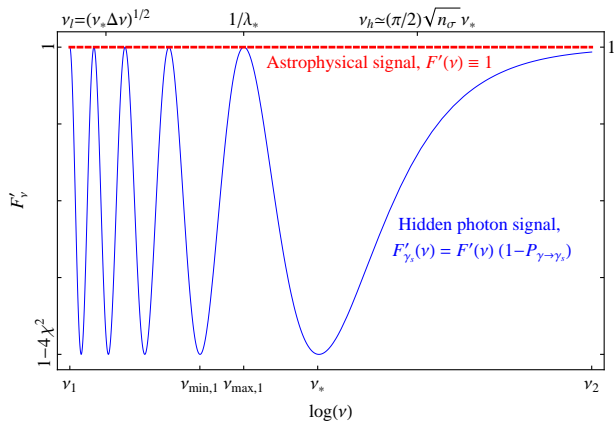


FIG. 1. Modulation of an ideally modeled astrophysical signal,  $F'(\nu) \equiv 1$ , by the hidden photon oscillations. Measurements cover the  $[\nu_1; \nu_2]$  frequency range and are made with a spectral resolution of  $\Delta\nu$ . Oscillations occur at a constant wavelength  $\lambda_*$ . Detection of the hidden-photon signal can be made if  $\nu_1 \leq \nu_{\min,2}$  and  $\nu_2 \geq \nu_*$ . Effective measurements (using the full sensitivity of the data) can be performed if  $\nu_1 \leq \nu_\ell$  and  $\nu_2 \geq \nu_h$ . The spectral resolution must be better than  $\nu_*/4$ .

These limits are analyzed and presented in Fig. 2 for several existing and planned radioastronomical facilities, and for different types of astrophysical targets. In real experiments, the accessible mass ranges may be further limited by coherence effects and medium propagation as discussed in Sections II A and III. This is illustrated in Fig. 2 by comparing the accessible ranges of hidden-photon masses to the limits imposed by the homogeneous ISM and IGM suppression. The impact of the medium suppression can be alleviated at lower photon masses by free propagation through a homogeneous medium (also illustrated in Fig. 2), in addition to the favorable conditions that may exist for propagation through an inhomogeneous medium.

The sensitivity to  $\chi$  varies within the mass ranges described by Eqs. 13-14. The lowest hidden-photon mass  $m_{\gamma_s}^{\ell, \text{full}}$  for which a set of measurements made in the  $[\nu_1; \nu_2]$  frequency range is fully sensitive to  $\chi$  is set by the condition  $\nu_\ell = \nu_1$ , which corresponds to

$$m_{\gamma_s}^{\ell, \text{full}} = \frac{2\pi\nu_1}{(L\Delta\nu)^{1/2}} = \frac{1}{\sqrt{2}} \left( \frac{\Delta\nu}{\nu_1} \right)^{-1/2} m_{\gamma_s}^{\ell}. \quad (15)$$

The largest mass that can be detected with at the full sensitivity is then given by the condition  $\nu_h = \nu_2$ , resulting in

$$m_{\gamma_s}^{\text{u, full}} = 2\sqrt{2\pi} \left[ \frac{\nu_2}{L} \arcsin \left( \frac{1}{\sqrt{n_\sigma}} \right) \right]^{1/2}, \quad (16)$$

with  $m_{\gamma_s}^{\text{u, full}} = 2\pi(\nu_2/L)^{1/2}$  for  $n_\sigma = 1$  and  $m_{\gamma_s}^{\text{u, full}} \approx 2\sqrt{2\pi}(\nu_2/L)^{1/2}n_\sigma^{-1/4}$  for  $n_\sigma \geq 2$ . With this approxima-

tion,  $m_{\gamma_s}^{\text{u, full}}$  can be expressed through  $m_{\gamma_s}^{\ell}$

$$m_{\gamma_s}^{\text{u, full}} \approx \frac{1}{\sqrt{\pi}n_\sigma^{1/4}} \left( \frac{\nu_2}{\nu_1} \right)^{1/2} m_{\gamma_s}^{\ell}. \quad (17)$$

The mass limits described by Eqs. 13-16 can be used to estimate the frequency dependence (or, conversely, the hidden-photon mass dependence) of the sensitivity provided by a given set of measurements for detecting the hidden-photon signal.

Eqs. 15 and 16, in particular, can be used for experimental optimization by requiring that  $m_{\gamma_s}^{\text{u, full}} > m_{\gamma_s}^{\ell, \text{full}}$ , which corresponds to the inequality

$$\sqrt{\frac{2}{\pi}} \frac{1}{n_\sigma^{1/4}} \left( \frac{\nu_2}{\nu_1} \right)^{1/2} \left( \frac{\Delta\nu}{\nu_1} \right)^{1/2} > 1$$

and connects the main parameters of the observational setup. For the goal of extending hidden photon studies to progressively lower hidden-photon masses, the most efficient strategy would therefore be to reduce  $\nu_1$ . Improving the frequency spacing can result in producing a progressively larger number of datapoints that could not be used for probing higher hidden-photon masses. Hence the overall range of full sensitivity of a given experimental setup would be reduced in this case.

## B. Sensitivity for the mixing angle $\chi$

The amplitude term  $a_\chi$  of  $P_{\gamma \rightarrow \gamma_s}$  implies that an  $n_\sigma$  bound on  $\chi \approx \sqrt{n_\sigma \sigma_{\text{rms}}}/2$  can be obtained from multi-frequency flux density measurements. For  $N$  individual flux density measurements with fractional errors  $\sigma_i$ ,  $\sigma_{\text{rms}} = \left( \sum_{i=1}^N \sigma_i^2 \right)^{1/2} / N \approx \sigma / N^{1/2}$  (if  $\sigma_i \approx \sigma$  for all  $i = 1, \dots, N$ ). One can assume, as an example, that the astrophysical signal from a target object can be described by a simple power-law spectrum  $F(\nu) = F_r(\nu/\nu_r)^\alpha$  and that the frequency dependence of the errors on flux density measurements changes can also be described by a power-law dependence  $\sigma(\nu) = \sigma_r(\nu/\nu_r)^\beta$  (here,  $F_r$  and  $\sigma_r$  refer to a flux density and its associated error, measured at an arbitrary reference frequency  $\nu_r$  chosen inside the relevant frequency range).

With these assumptions, measurements over the entire relevant frequency range  $[\nu_{\ell'}; \nu_{h'}]$  can be described by a characteristic signal-to-noise ratio

$$\hat{S} = \frac{1}{\nu_{h'} - \nu_{\ell'}} \int_{\nu_{\ell'}}^{\nu_{h'}} \frac{F(\nu)}{\sigma(\nu)} d\nu = \frac{F_r}{\sigma_r \nu_r^\xi} \frac{\nu_{h'}^{\xi+1} - \nu_{\ell'}^{\xi+1}}{(\xi+1)(\nu_{h'} - \nu_{\ell'})}, \quad (18)$$

where  $\xi = \alpha - \beta$  and the integration limits are given by  $\nu_{\ell'} = \max(\nu_1, \nu_\ell)$  and  $\nu_{h'} = \min(\nu_2, \nu_h)$ . At a frequency spacing  $\Delta\nu$ , the number of measurements contributing to the detection is  $N_{\text{mes}} = (\nu_{h'} - \nu_{\ell'})/\Delta\nu$ , hence the effective cumulative signal-to-noise ratio of the data set

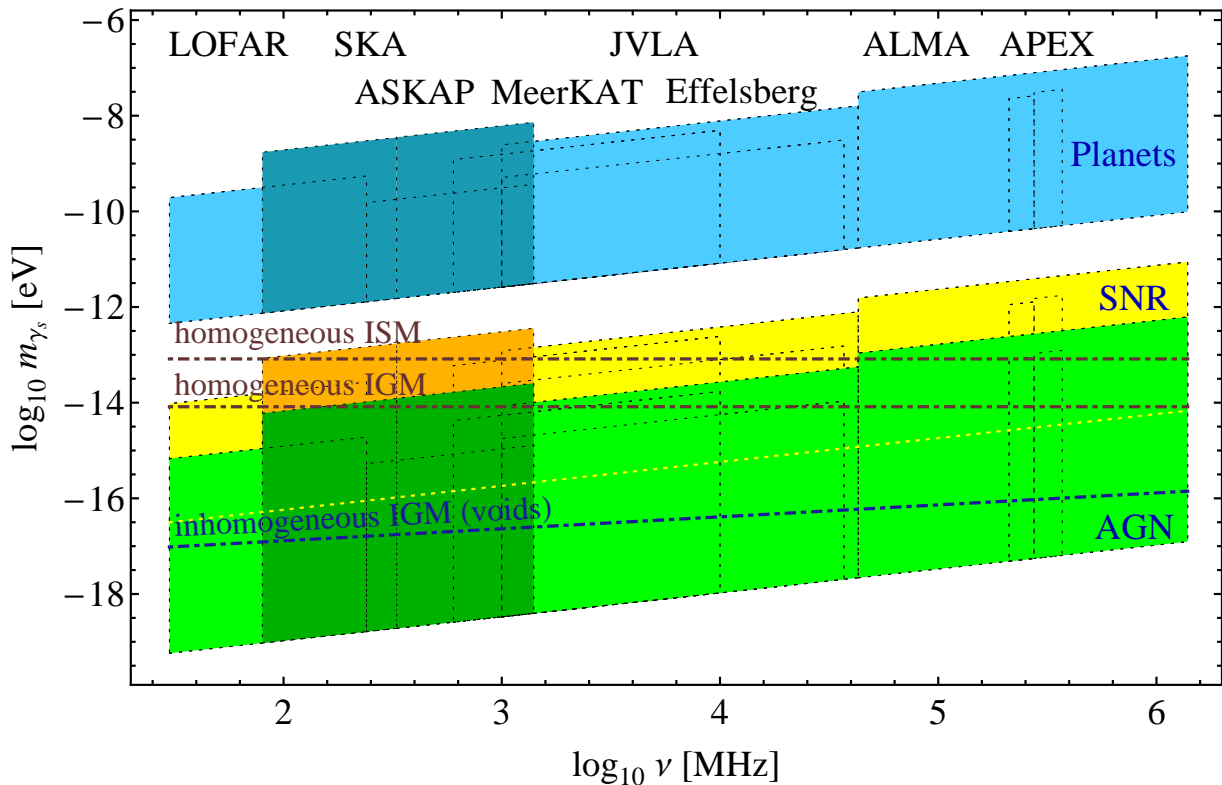


FIG. 2. Ranges of hidden-photon mass,  $m_{\gamma_s}$ , that can be probed with various radio astronomical instruments at different observing frequencies. The mass ranges are calculated for measurements done with planets (blue shades), supernovae remnants (yellow shades) and active galactic nuclei (green shades). For each individual color, darker shades mark the mass ranges accessible to measurements with the first and second phases of Square Kilometer Array (SKA). The calculations are made assuming typical instrumental setups and generic ranges of distances to planets (0.5–10 au), supernova remnants (1–10 kpc) and active galaxies (0.02–3 Gpc). Brown dot-dashed lines mark the lower limits on detectable mass imposed by homogeneous ISM and IGM suppression. The dashed blue line illustrates the lower limit on detectable mass arising from propagation through an inhomogeneous IGM containing large scale voids (for the assumed void diameter of 100 Mpc).

is  $\tilde{S} = N_{\text{mes}}^{1/2} \hat{S}$ . Recalling that, after accounting for the astrophysical signal,  $\tilde{S} \approx 1/\sigma_{\text{rms}}$  gives an estimate of the lowest achievable bound on the hidden photon coupling

$$\chi_{\text{low}} = \left( \frac{\sigma_r \nu_r^\xi (\xi + 1) (\nu_{h'} - \nu_{\ell'})^{1/2} (\Delta\nu)^{1/2}}{4F_r \nu_{h'}^{\xi+1} - \nu_{\ell'}^{\xi+1}} \right)^{1/2}. \quad (19)$$

The bound  $\chi_{\text{low}}$  remains constant for hidden photon masses  $m_{\gamma_s}^{\ell, \text{full}} \leq m_{\gamma_s} \leq m_{\gamma_s}^{u, \text{full}}$  and decreases rapidly outside this mass range as a progressively larger fraction of the measured data points are rendered outside the useful ranges of frequencies.

Figure 3a presents limits  $\chi_{\text{low}}$  calculated for several existing and planned radio astronomical facilities and for measurements made with Mars (with  $F_r = 30$  Jy and  $\alpha = 0.7$  at  $\nu_r = 86$  GHz; [61]), the supernova remnant Cassiopeia A ( $F_r = 3000$  Jy,  $\sigma_{\text{rms}} = 100$  Jy,  $\nu_r = 1$  GHz,  $\alpha = -0.8$ ; [62]), and a fiducial compact AGN ( $F_r = 10$  Jy,  $\alpha = -0.1$ ,  $\nu_r = 5$  GHz) at a distance of 1 Gpc. These limits are obtained for the vacuum oscillation regime, without taking into account the potential medium sup-

pression at lower hidden photon masses. For each of the instruments included in the plot, conservative assumptions for generic technical parameters (summarized in Appendix B) have been made, hence the actual limits could be further improved by optimizing observations with a given telescope, for instance by increasing the spectral resolution of the measurements or applying accurate in-band (bandpass) calibration [63]. The figure clearly reflects the effect of improvements of  $\sigma_{\text{rms}}$  (factor of  $\sim 10$ ) and  $\Delta\nu/\nu$  (factor of  $\sim 100$ ) that will be provided by the JVLA and SKA precursors, as well as the extension (factor of  $\sim 10$ ) to lower frequencies provided by LOFAR.

### C. Source stacking

Since the frequency behavior of the hidden-photon signal is determined solely by the hidden-photon mass and the distance to the target object, signals from any number of objects with known distances can be stacked to-

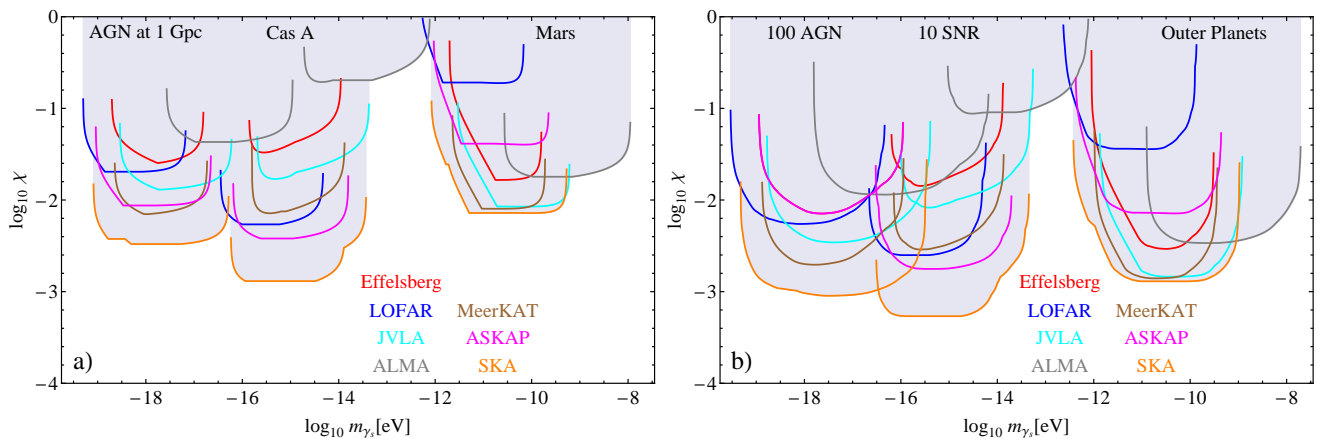


FIG. 3. Expected limits on  $\chi$  that can be obtained with different radio astronomical facilities and different astrophysical objects under the assumption that the measurements are not affected by the plasma propagation effects (vacuum oscillations). The limits are calculated assuming generic instrumental parameters and: (a) single target sources at distances of 1 Gpc, 3.4 kpc [60] and 2 au for the AGN, Cas A, and Mars, respectively, (b) stacked data limits obtained from simulated populations of 100 AGN ( $L=0.02\text{--}3$  Gpc,  $F=1\text{--}30$  Jy), 10 SNR ( $L=1\text{--}10$  kpc,  $F=10\text{--}100$  Jy) and 100 measurements made for the outer planets ( $L=0.5\text{--}10$  au,  $F=10\text{--}200$  Jy), with  $\gamma = -2$  used for all three populations.

gether to improve the resulting bound on the coupling constant. For the stacking, a suitable reference distance  $L'$  can be chosen, yielding for each object located at a distance  $L$  a modification of observed frequency  $\nu' = \nu(L'/L)$ .

If all of the stacked sources have the same spectra and distances, stacking of  $N_{\text{obj}}$  objects will lead to a  $N_{\text{obj}}^{1/4}$  improvement of  $\chi_{\text{low}}$ . Let the stacked objects be drawn from a population with a uniform spatial density over distances  $[L_{\text{min}}; L_{\text{max}}]$ , similar spectral indices, and an observed source count,  $N(F) = n(F_r)(F/F_r)^\gamma$  over a range of flux densities  $[F_{\text{min}}; F_{\text{max}}]$ .

In this case, stacking of  $N_{\text{obj}}$  spectra (each obtained with the same observational apparatus as described above) would yield a bound

$$\chi_{\text{stack}} = \chi_{\text{low}} N(\hat{F})^{-1/4}, \quad (20)$$

where  $\hat{F}$  is estimated at a frequency  $\hat{\nu}$  at which the signal-to-noise ratio  $\hat{S}$  is achieved. Calculation of  $\hat{S}$  may now involve different integration limits, as the frequencies  $\nu_\ell$  and  $\nu_h$  must be calculated for a characteristic distance  $\hat{L}$ . This distance is given by  $[(L_{\text{max}}^2 + L_{\text{min}}^2)/2]^{1/2}$  for planets and Galactic objects and by  $[(L_{\text{max}}^3 + L_{\text{min}}^3)/2]^{1/3}$  for extragalactic objects.

For the source and observation properties specified by  $F(\nu)$  and  $\sigma(\nu)$  (see Sect. III B),  $\hat{\nu} = \nu_r(\hat{S}\sigma_r/F_r)^{1/\xi}$ , giving  $\hat{F} = F_r^{1-\alpha/\xi}(\hat{S}\sigma_r)^{\alpha/\xi}$ . Consequently,  $N(\hat{F}) = n(F_r)(\hat{F}/F_r)^\gamma$ , where  $n(F_r) = N_{\text{obj}}F_r^\gamma(1+\gamma)\left(F_{\text{max}}^{1+\gamma} - F_{\text{min}}^{1+\gamma}\right)^{-1}$ .

Potential improvements of source stacking are illustrated in Fig. 3b which shows the limits on  $\chi$  that can be achieved by stacking together measurements made for 100 AGN, 10 SNR, and 100 measurements obtained for

different outer planets of the Solar System. Improvements in both  $\chi$  and the range of accessible hidden-photon mass are visible, compared to the single object limits in Fig 3a. The predictions for best cumulative limits from radio measurements in the entire 30 MHz to 1400 GHz range are compared in Fig. 4 to the bounds derived from other experiments and observations.

The potential effect of propagation through refractive media on the hidden-photon limits is illustrated in Figure 5 for three different cases describing the minimum values of the plasma density,  $n_{e,\text{min}}(l)$ , as a function of distance,  $l$ , along the propagation path. The three scenarios for  $n_{e,\text{min}}(l)$  are adopted here solely to assess the potential range of possible outcomes of the propagation of the hidden-photon signal through refractive media.

In all three scenarios,  $n_{e,\text{min}}(1 \text{ kpc}) = 10^{-5} \text{ cm}^{-3}$  is adopted, implying effectively that the LOS paths for galactic objects cross at least one of the galactic “mini void” regions. The worst case scenario assumes that the photon signal from extragalactic objects propagates mostly through galactic ISM, *i.e.*, not crossing large patches of IGM. In this case,  $n_{e,\text{min}}$  decreases from  $10^{-5} \text{ cm}^{-3}$  at  $l = 1 \text{ kpc}$  to  $10^{-7} \text{ cm}^{-3}$  at  $l = 3 \text{ Gpc}$  implying that, for more distant objects, the LOS path has a progressively larger probability to cross lower density IGM regions. The average case corresponds to propagation through typical IGM resulting in a  $n_{e,\text{min}} \sim 10^{-5}\text{--}10^{-8} \text{ cm}^{-3}$  range of densities. The best case allows for propagation through cosmic voids, with the corresponding  $n_{e,\text{min}} \sim 10^{-5}\text{--}10^{-10} \text{ cm}^{-3}$ . For the planets, the densities of 50, 30, and  $10 \text{ cm}^{-3}$  (measured at 1 au and scaling  $\propto (l/1 \text{ au})^{-2}$ ) have been adopted for the respective scenarios, based on measurements from [64].

The effects of resonant enhancement and medium suppression are clearly visible in the modified limits shown in



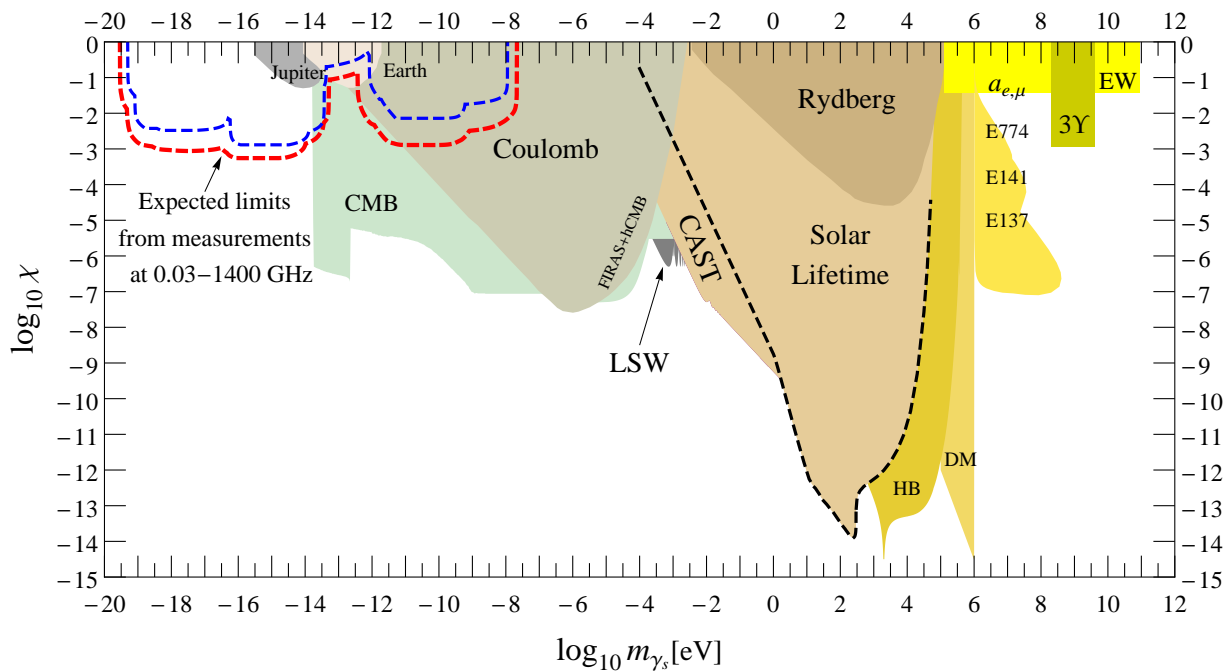


FIG. 4. Compound limits on  $\chi$  expected to be achievable from observations at 0.03–1400 GHz compared with the limits obtained presently with other facilities and experiments [7, and references therein]. The limits from single object (blue) and multiple object stacking (red) are shown. Radio observations (particularly at frequencies below 40 GHz) will provide a unique probe for the hidden photon with masses below  $10^{-14}$  eV and extending down to  $\sim 10^{-17}$  eV where the measurements are likely to be limited by the medium suppression of the hidden-photon signal in the IGM plasma as described in sections II B–II C.

Fig. 5. Assuming that the best case scenarios would apply for the majority of the lines of sight (since it is likely that a photon beam from a distant galaxy crosses one or more rarefied IGM or void regions), it is reasonable to conclude that the medium suppression would reduce the detectable  $\chi$  to  $\geq 0.01$  only for estimates made for  $m_{\gamma_s} \lesssim 10^{-17}$  eV. Above this mass, the propagation effects should not pose severe problems for constraining  $\chi$  (and they indeed may even play a constructive role at least for some fraction of the photon mass range).

#### D. Detection of periodic modulations

The modulations induced by the hidden-photon signal on the broad-band spectrum of an astrophysical object can be best detected in the wavelength domain, where the modulation is sinusoidal, with the period given by  $\lambda_*$ . A fast Fourier transform (FFT) can be applied for searches in the data with dense and uniform coverage of wavelength space. For sparsely sampled data, epoch folding [65] or generic uniformity tests such as the Rayleigh test [66] or  $Z_m^2$  test [67] can be applied.

These searches employ Eq. 11 with the  $C_{\mathcal{M}} = 1$  normalization of the residual flux density, which yields a functional form

$$f_\lambda = f_* [1 + a_* \sin(\omega_* \lambda + \phi_0)] \quad (21)$$

of the periodic signal to be searched for. Assuming that the residual errors after the normalization are  $\delta_\lambda = \sigma_{\text{rms}}/C_{\mathcal{M}}$ , the parameters of the functional form are related to the properties of the hidden-photon signal as follows:  $f_* = 1 - a_\chi/2 + \delta_\lambda$ ,  $a_* = a_\chi/(2f_*)$ ,  $\omega_* = \pi\nu_*$ ,  $\phi_0 = \pi/2$ . Appendix A provides specific details of application of three different methods (FFT, epoch folding and generic uniformity tests) to searches for periodic signals due to hidden photon oscillations.

## IV. DISCUSSION

The analysis described above demonstrates principal feasibility of searching for a hidden-photon signal in broad-band radio spectra of cosmic radio sources, with galactic supernova remnants and radio-loud AGN presenting the best opportunity for extending the measurements below the hidden-photon mass of  $10^{-14}$  eV, where essentially no measurements have been previously made.

The mass ranges and kinetic mixing limits accessible for these potential searches are determined by several factors, including the oscillation and coherence lengths of the hidden-photon signal, the instrumental bandwidth and resolution, as well as the plasma density changes along the line-of-sight path to the source of the photons. The combined effect of the signal coherence and oscillation length is expected to limit the searches to hidden-

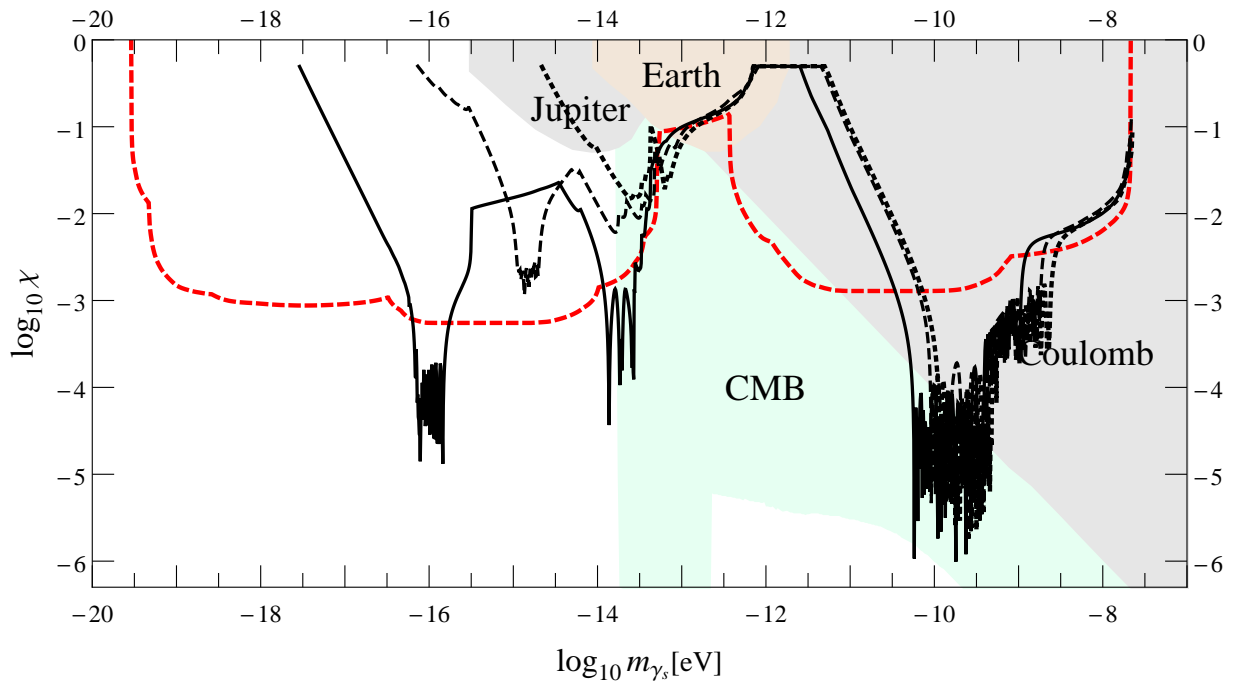


FIG. 5. Modifications of the combined limits on  $\chi$  due to propagation through refractive media. The dashed red line shows the limits predicted for object stacking observations under the vacuum condition (the same as the dashed red line in Fig. 4). The best (solid black), average (dashed black) and worst (dotted black) propagation scenarios illustrate potential effects of the ISM and IGM plasma for constraining the hidden-photon signal. For the best case scenario, the effect of resonant enhancement is visible. The medium suppression affects strongly the limits on  $\chi$  for hidden-photon masses below  $\sim 10^{-17}$  eV.

photon masses  $\gtrsim 10^{-19}$  eV, while the limits imposed by the propagation through the cosmic plasma may increase this limit up to  $\sim 10^{-17}$  eV.

Bandwidth and spectral resolution of the existing and planned radio astronomical facilities can support searches for hidden photons with masses well below  $10^{-20}$  eV. The limiting instrumental aspect is the accuracy of amplitude calibration of radio receiver, which may limit plausible constraints on kinetic mixing to  $\chi \approx 10^{-3}$ . This problem may be alleviated by the advent of ultra broadband receivers supporting in-band measurements across bandwidths in excess of 1 GHz. For this type of measurements, accurate bandpass calibration could deliver in-band amplitude accuracy of  $\geq 0.01\%$ , thus potentially further lowering the limits on the kinetic mixing by at least an order of magnitude.

For hidden-photon searches based on such in-band measurements, a combination of targets located at significantly different distances can be employed, profiting from the distance scaling of the hidden-photon signal. This ensures that any oscillatory pattern associated with a specific photon mass will be detectable only in one of the two measurements. This is realized for two objects at a distance ratio of  $L_2/L_1 (L_2 > L_1) \geq (\pi^2/4)(n_\sigma/\delta_\nu)$ , where  $\delta_\nu$  is the fractional spectral resolution of the measurements. With such arrangements, the upper limit for an amplitude of a periodic oscillation in the bandpass

obtained by dividing one of the two measured signals by the other would enable constraining  $\chi$  for the ranges of photon mass probed with either of the two targets.

The effect of propagation on the sensitivity introduces a dependence on the assumed electron density  $n_e$  of the intervening medium and therefore on the line of sight. For galactic sources, estimates of  $n_e$  at a specific line of sight can be obtained from pulsar dispersion measurements [52, 53]. Optical hydrogen absorption lines can be used for assessing the line-of-sight structure of the IGM [68], which can be applied for measurements in individual extragalactic targets. The situation may improve substantially after the large-scale HI surveys planned at the LOFAR, MeerKAT, ASKAP and the SKA [69–72] would deliver a very detailed picture of the IGM up to very high redshifts.

In the absence of information about the plasma properties on individual lines of sight, a potential remedy for the object stacking would be to make generic assumptions on the minimum plasma density as a function of distances to individual targets (similarly to the approach employed in Section III C). Despite being inherently imprecise, this approach should still enable improving the constraints obtained on  $\chi$  from object stacking.

Data from the next generation of large scale continuum and spectral line surveys at radio wavelengths will provide sufficiently accurate information about the broad-

band continuum, line-of-sight distribution of the IGM, and distances to many thousands of extragalactic radio sources. This will make object stacking the tool of choice for the hidden-photon searches in the radio regime and will certainly lead to strong improvements of the limits obtained from radio data on the kinetic mixing of hidden photons in the  $10^{-14}$ – $10^{-17}$  eV mass range.

## ACKNOWLEDGMENTS

We kindly acknowledge helpful discussions with Alessandro Mirizzi, Andreas Ringwald, and Günter Sigl. A.P.L. acknowledges support from the Collaborative Research Center (Sonderforschungsbereich) SFB 676 “Particles, Strings, and the Early Universe” funded by the German Research Society (Deutsche Forschungsgemeinschaft, DFG).

## Appendix A: Analysis techniques for periodic signals

### 1. FFT searches

An FFT search can be employed effectively for recovering the hidden photon signal, if measurements are made in a frequency range  $[\nu_1; \nu_2]$ , corresponding to a wavelength range  $\Lambda = \lambda_1 - \lambda_2$ . The measurements are assumed to be sampled densely enough to be binned into  $n_b = 2^m$  bins, with each bin described by the bin flux density  $f_i$  and its associated error  $\delta_i$ . This situation can be realized, for instance, for observations with high spectral resolution (e.g., with LOFAR, JVLA, or ALMA) applied to search for hidden photons with  $m_{\gamma_s} > 2\pi\sqrt{\nu_2/L}$ , for which  $\nu_\star > \nu_2$ . The resulting  $2m - 1$  Fourier coefficients are given by

$$|a_i|^2 = \sum_{j=1}^{n_b} f_j \exp(i\omega_i \lambda_j), \quad (\text{A1})$$

where  $\lambda_j = (j - 1/2)\Lambda/n_b$  is the arithmetic mean wavelength of the  $j^{\text{th}}$  bin and  $f_j$  is the respective bin-averaged flux density. The corresponding power spectrum  $w_i$  is given by

$$w_i = 2|a_i|^2/F_{\text{tot}}, \quad (\text{A2})$$

where  $F_{\text{tot}} = \sum_{j=1}^{n_b} f_j$  is the total flux density in the bins. The average power spectrum contribution from the measurement noise is accounted for by the term

$$\tilde{\delta} = \frac{1}{n_b} \sum_{i=1}^{n_b} \delta_i^2. \quad (\text{A3})$$

Adding the noise contribution and taking into account frequency dependence of  $|a_i|^2$  [65], the average power in the  $i^{\text{th}}$  bin can be written as

$$\langle w_i \rangle = \frac{\xi_\omega F_{\text{tot}}}{2} \left( \frac{a_\star \sin \varphi_i}{\varphi_i} \right)^2 + \tilde{\delta}, \quad (\text{A4})$$

where  $\varphi_i = \pi i/(2n_b)$  and  $\xi_\omega = 0.773$  [65] is a correction factor taking into account the finite bin width. Reaching, in a given bin, a desired confidence level,  $c$  (in percent), of detection of the oscillations, implies  $\langle w_i \rangle \geq w_0$ , where  $w_0$  is derived from the  $\chi^2$  probability distribution,  $p_2(\chi^2)$ , with two degrees of freedom, requiring that

$$1 - c/100 = (\Lambda/\lambda_\star) \int_{w_0}^{\infty} p_2(\chi^2) d\chi^2. \quad (\text{A5})$$

If a signal is detected, the amplitude  $a_\star$  (and consequently, the kinetic mixing parameter  $a_\chi$ ) can be obtained by requiring that

$$c/100 = \int_{w_a}^{\infty} p_2(\chi^2) d\chi^2, \quad (\text{A6})$$

with  $w_a = w_0 - \langle w_i \rangle + \tilde{\delta}/2$ .

### 2. Epoch folding

If the data are not homogeneously sampled across the measured wavelength domain  $\Lambda$  but still can be divided into phase bins of size  $\leq \Delta\nu/\nu_2$  (thus giving  $n_\phi \geq 2\nu_2(\nu_2 - \nu_1)/(\nu_1 \Delta\nu)$  phase bins), epoch folding [cf., 65, 73] can be effectively performed in order to search for all hidden-photon masses in the  $[m_{\gamma_s}^l; m_{\gamma_s}^u]$  range. After epoch folding with a given trial wavelength  $\lambda'$ , each bin is characterized by the bin flux density  $f_i$  and its associated error  $\delta_i$ . The significance of the signal can be assessed using the statistics  $s = \sum_{i=1}^{n_\phi-1} (f_i - \tilde{f})^2/\delta_i^2$ , where  $\tilde{f} = F_{\text{tot}}/n_\phi$ . For the same assumptions as used above for the FFT searches, the mean value of the statistics is given by

$$\langle s \rangle = \frac{\xi_\phi F_{\text{tot}}}{2} \left( \frac{a_\star \sin \varphi}{\varphi} \right)^2 + \frac{\tilde{\delta}}{2}, \quad (\text{A7})$$

with  $\varphi = \pi/n_\phi$  and  $\xi_\phi = 0.935$  [65]. The sensitivity to oscillations is established at a confidence level  $c$  by requiring  $\langle s \rangle \geq s_0$  where  $s_0$  is obtained from the condition

$$1 - c/100 = (\Lambda/\lambda') \int_{s_0}^{\infty} p_{n_\phi-1}(\chi^2) d\chi. \quad (\text{A8})$$

Similarly, the amplitude of the detected signal can be estimated from

$$c/100 = \int_{s_a}^{\infty} p_{n_\phi-1}(\chi^2) d\chi^2, \quad (\text{A9})$$

where  $s_a = s_0 - \langle s \rangle + \tilde{\delta}/2$ .

### 3. Generic uniformity tests

For poorly and unevenly sampled data, generic uniformity tests such as the Rayleigh test [66, 73, 74], the  $Z_m^2$

TABLE IV. Generic technical parameters of radio telescopes used in the calculations of sensitivity for  $\chi$  in the radio regime.

Telescope	$\nu_1$ [GHz]	$\nu_2$ [GHz]	$N_{\text{ch}}$	$\sigma_r$ [Jy]	$\beta$
LOFAR	0.03	0.24	1000	0.3	-0.25
SKA <sub>1</sub>	0.08	0.33	5000	0.04	-0.1
ASKAP	0.1	1.4	2000	0.1	-0.25
SKA <sub>2</sub>	0.3	3.0	5000	0.04	0.1
MeerKAT	0.6	10	200	0.03	0.25
Effelsberg	0.3	37	40	0.1	0.25
JVLA	0.3	43	500	0.1	0.25
APEX	170	410	4000	10	0.25
ALMA	86	1389	5000	1	0.25

test [67] or the  $H$ -test [75] can be applied, relieving also the requirement to bin the data before searching for a periodic signal.

Similar to the case of epoch folding, the data consisting of  $n$  flux density measurements have to be first normalized by a factor of  $f_{\text{min}} = \min(f_i)$  and folded with a trial wavelength  $\lambda'$ , yielding a set of amplitudes  $f'_i = f_i/f_{\text{min}}$  and phases  $\phi_i$ , with  $i = 1, \dots, n$ . Calculation of the respective trigonometric moments is done using the terms  $f'_i \cos \phi_i$  and  $f'_i \sin \phi_i$ , so that the resulting Rayleigh power becomes

$$nR^2 = \frac{1}{n} \left[ \left( \sum_{i=1}^n f'_i \cos \phi_i \right)^2 + \left( \sum_{i=1}^n f'_i \sin \phi_i \right)^2 \right]. \quad (\text{A10})$$

Similar modification should be done to the trigonometric

moments entering the  $Z_m^2$  statistics

$$Z_m^2 = \frac{2}{n} \sum_{j=1}^m \left\{ \left[ \sum_{i=1}^n f'_i \cos(j \phi_i) \right]^2 + \left[ \sum_{i=1}^n f'_i \sin(j \phi_i) \right]^2 \right\}. \quad (\text{A11})$$

The resulting calculated powers  $2nR^2$  and  $Z_m^2$  should be tested against  $\chi^2$  distributions  $p_2(\chi^2)$  and  $p_{2m}(\chi^2)$ , respectively. Adopting the same approach as for the epoch folding, these values will yield confidence limits for detecting a periodic signal with the wavelength  $\lambda'$ .

## Appendix B: Basic technical characteristics of simulated radio observations

Table IV describes general technical parameters adopted for simulating observations with the radio telescopes used for the predictions of the hidden-photon mass ranges and the limits on  $\chi$  from measurements in the radio regime at frequencies of 0.03–1400 GHz. The parameters presented in the table are: the lowest  $\nu_1$  and highest  $\nu_2$  observing frequencies, the number of measurements,  $N_{\text{ch}}$ , available within the observing range, the r.m.s. noise,  $\sigma_r$  of a single measurement at the reference frequency  $\nu_r$ , and the power index  $\beta$  describing the frequency dependence of the r.m.s. noise. The parameter values given in Table IV provide only basic benchmark description of technical capabilities of the individual telescopes. Conservative estimates have been adopted for the number of spectral channels and the r.m.s. noise (assuming typical “shallow” survey observations), and these values can be improved by one or more orders of magnitude by employing full correlator capabilities and dedicated targeted observations.

- 
- [1] G. Jungman, M. Kamionkowski, and K. Griest, Phys. Rep. **267**, 195 (1996), hep-ph/9506380.
- [2] G. Bertone, D. Hooper, and J. Silk, Phys. Rep. **405**, 279 (2005), hep-ph/0404175.
- [3] G. Bertone, Nature **468**, 389 (2010), 1011.3532.
- [4] L. B. Okun, ZhETF **83**, 892 (1982).
- [5] L. Bergström, Reports on Progress in Physics **63**, 793 (2000), arXiv:hep-ph/0002126.
- [6] M. Ahlers, J. Jaeckel, J. Redondo, and A. Ringwald, Phys. Rev. D **78**, 075005 (2008), arXiv:0807.4143 [hep-ph].
- [7] J. Jaeckel and A. Ringwald, ARNPS **60**, 405 (2010), arXiv:1002.0329 [hep-ph].
- [8] A. Ringwald, ArXiv e-prints (2012), arXiv:1210.5081 [hep-ph].
- [9] J. Jaeckel, E. Massó, J. Redondo, A. Ringwald, and F. Takahashi, Phys. Rev. D **75**, 013004 (2007), arXiv:hep-ph/0610203.
- [10] G. Raffelt and L. Stodolsky, Phys. Rev. D **37**, 1237 (1988).
- [11] E. Zavattini, G. Zavattini, G. Ruoso, E. Polacco, E. Milotti, M. Karuza, U. Gastaldi, G. di Domenico, F. Della Valle, R. Cimino, S. Carusotto, G. Cantatore, and M. Bregant, Phys. Rev. Lett. **96**, 110406 (2006), arXiv:hep-ex/0507107.
- [12] M. Ahlers, H. Gies, J. Jaeckel, J. Redondo, and A. Ringwald, Phys. Rev. D **76**, 115005 (2007), arXiv:0706.2836 [hep-ph].
- [13] J. Redondo and M. Postma, J. Cosmology Astropart. Phys. **2**, 005 (2009), arXiv:0811.0326 [hep-ph].
- [14] P. Arias, D. Cadamuro, M. Goodsell, J. Jaeckel, J. Redondo, and A. Ringwald, J. Cosmology Astropart. Phys. **6**, 013 (2012), arXiv:1201.5902 [hep-ph].
- [15] B. Holdom, Physics Letters B **166**, 196 (1986).
- [16] J. Jaeckel, J. Redondo, and A. Ringwald, Phys. Rev. Lett. **101**, 131801 (2008), arXiv:0804.4157.
- [17] J. Redondo, J. Cosmology Astropart. Phys. **7**, 008 (2008), arXiv:0801.1527 [hep-ph].

- [18] K. R. Dienes, C. Kolda, and J. March-Russell, Nuclear Physics B **492**, 104 (1997), arXiv:hep-ph/9610479.
- [19] S. A. Abel, M. D. Goodsell, J. Jaeckel, V. V. Khoze, and A. Ringwald, Journal of High Energy Physics **7**, 124 (2008), arXiv:0803.1449 [hep-ph].
- [20] S. A. Abel, J. Jaeckel, V. V. Khoze, and A. Ringwald, Physics Letters B **666**, 66 (2008), arXiv:hep-ph/0608248.
- [21] M. Goodsell, J. Jaeckel, J. Redondo, and A. Ringwald, Journal of High Energy Physics **11**, 027 (2009), arXiv:0909.0515 [hep-ph].
- [22] M. Cicoli, M. Goodsell, J. Jaeckel, and A. Ringwald, Journal of High Energy Physics **7**, 114 (2011), arXiv:1103.3705 [hep-th].
- [23] S. J. Asztalos, G. Carosi, C. Hagmann, D. Kinion, K. van Bibber, M. Hotz, L. J. Rosenberg, G. Rybka, J. Hoskins, J. Hwang, P. Sikivie, D. B. Tanner, R. Bradley, J. Clarke, and ADMX Collaboration, Physical Review Letters **104**, 041301 (2010), arXiv:0910.5914 [astro-ph.CO].
- [24] P. Sikivie, ArXiv e-prints (2010), arXiv:1009.0762 [hep-ph].
- [25] O. K. Baker, M. Betz, F. Caspers, J. Jaeckel, A. Lindner, A. Ringwald, Y. Semertzidis, P. Sikivie, and K. Zioutas, Phys. Rev. D **85**, 035018 (2012), arXiv:1110.2180 [physics.ins-det].
- [26] A. Afanasev, O. K. Baker, K. B. Beard, G. Biallas, J. Boyce, M. Minarni, R. Ramdon, M. Shinn, and P. Slocum, in *American Institute of Physics Conference Series*, Vol. 1200, edited by G. Alverson, P. Nath, and B. Nelson (2010) pp. 1081–1084.
- [27] K. Ehret, M. Frede, S. Ghazaryan, M. Hildebrandt, E.-A. Knabbe, D. Kracht, A. Lindner, J. List, T. Meier, N. Meyer, D. Notz, J. Redondo, A. Ringwald, G. Wiedemann, and B. Willke, Phys. Lett. B **689**, 149 (2010), arXiv:1004.1313 [hep-ex].
- [28] D. Cadamuro and J. Redondo, ArXiv:hep-ph/1010.4689 (2010), arXiv:1010.4689 [hep-ph].
- [29] A. Wagner, G. Rybka, M. Hotz, L. J. Rosenberg, S. J. Asztalos, G. Carosi, C. Hagmann, D. Kinion, K. van Bibber, J. Hoskins, C. Martin, P. Sikivie, D. B. Tanner, R. Bradley, and J. Clarke, Physical Review Letters **105**, 171801 (2010), arXiv:1007.3766 [hep-ex].
- [30] S. Andreas, C. Niebuhr, and A. Ringwald, ArXiv e-prints (2012), arXiv:1209.6083 [hep-ph].
- [31] M. Betz and F. Caspers, ArXiv e-prints (2012), arXiv:1207.3275 [physics.ins-det].
- [32] H.-S. Zechlin, D. Horns, and J. Redondo, in *American Institute of Physics Conference Series*, Vol. 1085, edited by F. A. Aharonian, W. Hofmann, & F. Rieger (2008) pp. 727–730, arXiv:0810.5501.
- [33] A. Mirizzi, J. Redondo, and G. Sigl, JCAP **3**, 26 (2009), arXiv:0901.0014 [hep-ph].
- [34] P. Arias, J. Jaeckel, J. Redondo, and A. Ringwald, Phys. Rev. D **82**, 115018 (2010), arXiv:1009.4875 [hep-ph].
- [35] J. Redondo, ArXiv:hep-ph/1002.0447 (2010), arXiv:1002.0447 [hep-ph].
- [36] J. Redondo and A. Ringwald, Contemporary Physics **52**, 211 (2011), arXiv:1011.3741 [hep-ph].
- [37] M. Schwarz, A. Lindner, J. Redondo, A. Ringwald, and G. Wiedemann, ArXiv e-prints (2012), arXiv:1111.5797 [astro-ph.IM].
- [38] A. S. Goldhaber and M. M. Nieto, Reviews of Modern Physics **43**, 277 (1971).
- [39]  $1 \text{ Jy} = 10^{-26} \text{ J m}^{-2} \text{ s}^{-1} \text{ Hz}^{-1}$ .
- [40] Square Kilometer Array, a next generation radio telescope that will provide about a two orders of magnitude improvement in imaging sensitivity and surveying speed for radio observations in the 0.3–20 GHz frequency range; <http://www.skatelescope.org>.
- [41] <http://www.ska.ac.za/meerkat>.
- [42] <http://www.atnf.csiro.au/SKA>.
- [43] J. W. M. Baars, R. Genzel, I. I. K. Pauliny-Toth, and A. Witzel, A&A **61**, 99 (1977).
- [44] T. K. Kuo and J. Pantaleone, Phys. Rev. D **39**, 1930 (1989).
- [45] S. Nussinov, Physics Letters B **63**, 201 (1976).
- [46] C. Giunti and C. W. Kim, Phys. Rev. D **58**, 017301 (1998), arXiv:hep-ph/9711363.
- [47] M. Meyer, Diploma thesis, University of Hamburg (2010).
- [48] K. M. Ferrière, Reviews of Modern Physics **73**, 1031 (2001), arXiv:astro-ph/0106359.
- [49] G. Hinshaw, J. L. Weiland, R. S. Hill, N. Odegard, D. Larson, C. L. Bennett, J. Dunkley, B. Gold, M. R. Greason, N. Jarosik, E. Komatsu, M. R. Nolta, L. Page, D. N. Spergel, E. Wollack, M. Halpern, A. Kogut, M. Limon, S. S. Meyer, G. S. Tucker, and E. L. Wright, ApJS **180**, 225 (2009), arXiv:0803.0732.
- [50] S. Gottlöber, E. L. Lokas, A. Klypin, and Y. Hoffman, MNRAS **344**, 715 (2003), arXiv:astro-ph/0305393.
- [51] A. V. Pynzar' and V. I. Shishov, Astronomy Reports **52**, 623 (2008).
- [52] J. H. Taylor and J. M. Cordes, ApJ **411**, 674 (1993).
- [53] J. M. Cordes and T. J. W. Lazio, ArXiv:astro-ph/0207156 (2002), arXiv:astro-ph/0207156.
- [54] M. Plionis and S. Basilakos, MNRAS **330**, 399 (2002), arXiv:astro-ph/0106491.
- [55] D. C. Pan, M. S. Vogeley, F. Hoyle, Y.-Y. Choi, and C. Park, MNRAS **421**, 926 (2012), arXiv:1103.4156 [astro-ph.CO].
- [56] A. V. Kravtsov, A. Klypin, and Y. Hoffman, ApJ **571**, 563 (2002), arXiv:astro-ph/0109077.
- [57] R. Cen, K. Nagamine, and J. P. Ostriker, ApJ **635**, 86 (2005), arXiv:astro-ph/0407143.
- [58] E. Komatsu, K. M. Smith, J. Dunkley, C. L. Bennett, B. Gold, G. Hinshaw, N. Jarosik, D. Larson, M. R. Nolta, L. Page, D. N. Spergel, M. Halpern, R. S. Hill, A. Kogut, M. Limon, S. S. Meyer, N. Odegard, G. S. Tucker, J. L. Weiland, E. Wollack, and E. L. Wright, ApJS **192**, 18 (2011), arXiv:1001.4538 [astro-ph.CO].
- [59] R. K. Sheth and R. van de Weygaert, MNRAS **350**, 517 (2004), arXiv:astro-ph/0311260.
- [60] R. A. Fesen, M. C. Hammell, J. Morse, R. A. Chevalier, K. J. Borkowski, M. A. Dopita, C. L. Gerardy, S. S. Lawrence, J. C. Raymond, and S. van den Bergh, ApJ **645**, 283 (2006), arXiv:astro-ph/0603371.
- [61] J. L. Weiland, N. Odegard, R. S. Hill, E. Wollack, G. Hinshaw, M. R. Greason, N. Jarosik, L. Page, C. L. Bennett, J. Dunkley, B. Gold, M. Halpern, A. Kogut, E. Komatsu, D. Larson, M. Limon, S. S. Meyer, M. R. Nolta, K. M. Smith, D. N. Spergel, G. S. Tucker, and E. L. Wright, ApJS **192**, 19 (2011), arXiv:1001.4731 [astro-ph.CO].

- [62] J. W. M. Baars, *A&A* **17**, 172 (1972).
- [63] B. Winkel, A. Kraus, and U. Bach, *A&A* **540**, A140 (2012), arXiv:1203.0741 [astro-ph.IM].
- [64] S. J. Tappin, *Planet. Space Sci.* **34**, 93 (1986).
- [65] D. A. Leahy, W. Darbro, R. F. Elsner, M. C. Weisskopf, S. Kahn, P. G. Sutherland, and J. E. Grindlay, *ApJ* **266**, 160 (1983).
- [66] K. T. S. Brazier, *MNRAS* **268**, 709 (1994).
- [67] R. Buccheri, K. Bennett, G. F. Bignami, J. B. G. M. Bloemen, V. Boriakoff, P. A. Caraveo, W. Hermsen, G. Kanbach, R. N. Manchester, J. L. Masnou, H. A. Mayer-Hasselwander, M. E. Ozel, J. A. Paul, B. Sacco, L. Scarsi, and A. W. Strong, *A&A* **128**, 245 (1983).
- [68] S. Caucci, S. Colombi, C. Pichon, E. Rollinde, P. Petitjean, and T. Sousbie, *MNRAS* **386**, 211 (2008).
- [69] F. B. Abdalla and S. Rawlings, *MNRAS* **360**, 27 (2005), arXiv:astro-ph/0411342.
- [70] A. R. Duffy, R. A. Battye, R. D. Davies, A. Moss, and P. N. Wilkinson, *MNRAS* **383**, 150 (2008), arXiv:0707.2316.
- [71] H. Röttgering, J. Afonso, P. Barthel, F. Batejat, P. Best, A. Bonafede, M. Brügger, G. Brunetti, K. Chyży, J. Conway, F. D. Gasperin, C. Ferrari, M. Haverkorn, G. Heald, M. Hoeft, N. Jackson, M. Jarvis, L. Ker, M. Lehnert, G. Macario, J. McKean, G. Miley, R. Morganti, T. Oosterloo, E. Orrù, R. Pizzo, D. Rafferty, A. Shulevski, C. Tasse, I. V. Bemmell, B. van der Tol, R. van Weeren, M. Verheijen, G. White, and M. Wise, *Journal of Astrophysics and Astronomy* **32**, 557 (2011), arXiv:1107.1606 [astro-ph.CO].
- [72] A. R. Duffy, M. J. Meyer, L. Staveley-Smith, M. Bernyk, D. J. Croton, B. S. Koribalski, D. Gerstmann, and S. Westerlund, *MNRAS* **426**, 3385 (2012), arXiv:1208.5592 [astro-ph.CO].
- [73] D. A. Leahy, R. F. Elsner, and M. C. Weisskopf, *ApJ* **272**, 256 (1983).
- [74] K. V. Mardia and P. E. Jupp, *Directional Statistics* (Wiley & Sons: Chichester, 2000).
- [75] O. C. de Jager, B. C. Raubenheimer, and J. W. H. Swanepoel, *A&A* **221**, 180 (1989).